Novel features of the α–β phase transition in quartz-type $FePO_4$ as evidenced by x-ray diffraction and lattice dynamics

2010 J. Phys.: Condens. Matter 22 225403

(http://iopscience.iop.org/0953-8984/22/22/225403)

J. Phys.: Condens. Matter **22** (2010) 225403 (10pp) doi:10.1088/0953-8984/22/22/225403

Novel features of the α–β phase transition in quartz-type $FePO_4$ as evidenced by x-ray diffraction and lattice dynamics

M Smirnov[1], N Mazhenov[2], N Aliouane[3] and P Saint-Grégoire[4,5]

[1] Physical Department of Saint-Petersburg State University, Petrodvoretz, 194508 St-Petersburg, Russia
[2] Karaganda Technical University, 100027 Karaganda, Kazakhstan
[3] Physics Department, Institute for Energy Technology, PO Box 40, NO-2027 Kjeller, Norway
[4] Department of Sciences and Arts, University of Nîmes, F-30021 Nîmes Cedex, France
[5] ICGM, PMOF, University of Montpellier 2, F-34095 Montpellier Cedex, France

E-mail: smirnomb@rambler.ru

Received 2 February 2010, in final form 21 April 2010
Published 20 May 2010
Online at stacks.iop.org/JPhysCM/22/225403

Abstract

We present novel results on the mechanism of the α–β structural phase transition (STP) occurring in $FePO_4$. High accuracy x-ray diffraction experiments followed by a structural analysis provide us with precise information on the thermal disorder change on different atomic sites. The data are analysed in the light of lattice dynamics simulation results. The rigid unit mode (RUM) approach of the dynamics simulation allows an understanding of the anisotropic displacement parameters (ADPs). Surprisingly, the role of critical fluctuations of the order parameter, in the sense of Landau and Lifshitz theory, appears not to be relevant in the case of this SPT and the understanding of the dynamics requires a knowledge and analysis of the microscopic details of the system.

(Some figures in this article are in colour only in the electronic version)

1. Introduction

Iron phosphate $FePO_4$ belongs to the family of ABO_4 compounds (A = Si, Ge, Al, Fe, Ga; B = Si, Ge, P, As) crystallizing in a quartz-like structure. Within this family, only quartz, berlinite ($AlPO_4$) and iron phosphate undergo the high-temperature α–β phase transition [1–5]. This structural phase transition (SPT) has attracted a great deal of attention because of related anomalies in the thermal expansion, elastic and optical properties [6]. Recent renewal of interest in the α–β SPT was inspired by the discovery of an incommensurate phase in quartz [7, 8] that has to be taken into account to understand the old problem of small-angle light-scattering anomalies [9–14].

The α–β SPT in $FePO_4$ stands out for its relatively high T_c value and for the highest volume increase. In $FePO_4$, the incommensurate state, intermediate between the α- and β-phases, also exists but within a temperature interval of 17 K [15], which is much wider than in quartz (1.5 K) [16, 17] and in berlinite (2.5 K) [18, 19]. This situation, together with data on the crystalline structure of iron phosphate, indicates that the phenomena occurring in this compound could be distinguished from those in quartz and berlinite.

In particular, concerning the SPT, tracing the structure variation during the α–β transformation is of crucial importance for understanding the microscopic mechanism. The aim of this paper is to focus on this question. Particular attention has been paid to the displacement parameters in iron phosphate at different temperatures in the α-and β-phases in order to understand the common features with quartz and berlinite and to reveal the origin of their striking dissimilarities.

This paper is organized as follows. In section 2, we give a summary of the results on anisotropic displacement parameters (ADPs) and on probability density functions (PDFs) in quartz and berlinite. We compare experimental results with simulations, in the framework of the problem of the order–disorder or displacive character of the transition. In section 3, we introduce the present experimental study and describe the

experimental conditions, methods used, results and discussions on the refinement of structural parameters and ADPs for $FePO_4$ in the α-and β-phases obtained from the analysis of synchrotron powder x-ray diffraction patterns. Finally, in section 4 we present our results on the lattice dynamics simulation performed to clarify the difference in ADPs which differ significantly in β-$FePO_4$ from those observed in quartz and berlinite. This allowed us to reveal the most unstable phonon modes determining the ADPs in β-$FePO_4$ and to explain the particularity of this compound.

2. Summary of the SPT mechanism in quartz and berlinite, and of the thermal disorder phenomena

A considerable amount of study has been devoted to anisotropic displacement parameters and to probability density functions in quartz and berlinite. It was found [20] that in quartz the ADPs for oxygen and silicon atoms in the directions closely related to the atomic displacements at the α–β transition show anomalous temperature dependence at the critical temperature. On heating, they sharply (almost spontaneously) increase by about 30%, and afterwards decrease immediately after the transition. Besides, it was shown that the PDFs for oxygen are eventually unimodal at all temperatures, but deviate considerably from the Gaussian distributions in the β-phase.

The origin of the non-Gaussian shape of the PDF distribution in the β-phase was elucidated owing to the results of molecular dynamics (MD) simulations [21]. It was discovered that the β-quartz structure, as it appears within the MD simulation, has a peculiar dynamical character. When averaged over a long time, the probability distribution mimics a displacive shift to the ordered β structure. However, averaging over a shorter time shows that atoms hop between the two equivalent α_1 and α_2 structures through anharmonic motions with a temperature-dependent correlation time. Thus, the non-Gaussian PDF distribution for the β-phase matches well with the superposition of two Gaussian distributions centred at positions corresponding to the α_1 and α_2 structures.

The experimental study of berlinite [22] did not reveal any marked difference as compared with quartz. The temperature dependences of the atomic position and ADPs were found to be strikingly similar to those in quartz. The ADP ellipsoids for Al and P are oriented with their largest axes parallel to the twofold axes at all temperatures. The Al–O and P–O bond lengths are nearly constant in temperature. The highly anisotropic mean square displacements of O atoms were found to increase markedly with increasing temperature, especially in a narrow interval just below the critical point. The similarities of α–β SPTs in quartz and in berlinite were confirmed by the results of the MD study [23], which revealed the same double-Gaussian shape of PDF distributions for all atoms in the β-phase of berlinite.

The structural aspects of the α–β transformation in $FePO_4$ were studied much less frequently. The neutron diffraction study [5] revealed that the behaviour of this crystal during the α–β transformation is distinct from those other ABO_4 homologues: the temperature-induced variations of the AO_4 and BO_4 tetrahedra tilting and the A–O–B angles are much larger and do not scale with the initial β-to-α distortion. The ADPs for $FePO_4$ were determined only for the room-temperature α-phase [2]. For β-$FePO_4$, only isotropic displacement parameters (IDP) were reported [5].

The present paper reports the refinement of structural parameters and ADPs for both α-and β-phases of $FePO_4$ obtained from the analysis of high resolution synchrotron powder x-ray diffraction patterns. The ADPs determined for β-$FePO_4$ differ significantly from those observed in quartz and berlinite. First of all, this concerns the orientations of ADP ellipsoids which do not correlate with atomic displacements dictated by a displacive mechanism of the α–β transformation.

The absence of such a correlation does not seem unbelievable if we adopt a new look at the mechanism of the α–β SPT in quartz-like crystals reported in [24]. The data obtained in that study by using neutron diffraction experiments and the reverse Monte Carlo method clearly showed that the structure of the high-temperature phase does not consist of domains of an ordered α structure, and does not involve the SiO_4 tetrahedra jumping between two orientations, as in a classical order–disorder phase transition. The interesting picture that emerged from the results of [24] showed that there is a much more thermally induced dynamic disorder than in either the classical soft-mode or the multi-domain models. This disorder sets in at temperatures considerably below T_c. The important finding was that this large dynamic disorder is due not to fluctuations of the order parameter itself, as in critical fluctuations, but to the excitation of new low-energy vibrations that are allowed to be excited as a result of the symmetry change associated with the phase transition.

From this point of view it can be suggested that the shape of the PDF distribution in the β-phase is not necessarily dictated by the order-parameter fluctuation. Our experimental data show that such a situation does occur in $FePO_4$. In order to verify this hypothesis, we performed lattice dynamics simulations, which allowed us to reveal the harmonically unstable phonon modes mostly contributing to the ADPs in β-$FePO_4$. The obtained results provide a tentative explanation of the particularity of α–β SPT in $FePO_4$ in the framework of the model proposed in [24]. The view presented in [24] and shared by the authors of this paper accounts for that a static or dynamic picture cannot easily be derived from diffraction data. A well-grounded self-consistent analysis should include the lattice dynamics consideration.

3. Experimental conditions, results and their discussion

3.1. Experimental conditions

Anhydrous $FePO_4$ was prepared from commercial (Aldrich) powder of $FePO_4{\cdot}2H_2O$ by annealing at about 670 K during 3 h. Recrystallization was performed with an additional annealing at 720 K during 6 h, leading to the optimal characteristics of the final powder (good crystallization and no parasite phase). The powder was then introduced into a silica capillary of 0.3 mm diameter. The x-ray diffraction pattern

Table 1. Unit cell parameters a and c (in Å) and fractional atomic coordinates for α-and β-phases of $FePO_4$.

		α-phase[a], $T = 300$ K		β-phase[b], $T = 1073$ K	
		XRD, this work	ND, [5]	XRD, this work	ND, [5]
a		5.0287(9)	5.0314(1)	5.1907(8)	5.1621(4)
c		11.2291(0)	11.2465(2)	11.4320(8)	11.366(1)
Fe	x	0.4568(1)	0.4564(3)	0.5	0.5
P	x	0.4595(3)	0.4545(6)	0.5	0.5
O1	x	0.4130(1)	0.4158(5)	0.421(4)	0.425(1)
	y	0.3121(9)	0.3195(4)	0.217(8)	0.222(3)
	z	0.3967(4)	0.3960(1)	0.589(3)	0.591(1)
O2	x	0.4113(8)	0.4099(5)		
	y	0.2673(7)	0.2621(4)		
	z	0.8738(1)	0.8760(1)		

[a] Trigonal: P3121, Fe: 3a sites (x, 0, 1/3), P: 3b sites (x, 0, 5/6), O1 and O2: 6c sites (x, y, z).
[b] Hexagonal: P6422, Fe: 3d sites (1/2, 0, 1/2), P: 3c sites (1/2, 0, 0), O: 12k sites (x, y, z).

was collected at 1073 K (i.e. about 90 K above the phase transition temperature to avoid the α-phase coexistence) using a synchrotron source (Dw 22 line at LURE, $\lambda = 0.6883$ Å in 2θ scan with a rotating sample). Typical data collection covered a range of $0.05 < \sin\theta/\lambda < 0.77$. The temperature stability was better than 0.5 K. A diffraction pattern was also recorded at room temperature in order to refine the structure of the α-phase. The Rietveld refinements were performed using the Fullprof-98 software [25], based on a full matrix least-squares program. The standard scattering lengths for Fe, P and O were used. The intensities were corrected for linear absorption with $\mu = 50.18$ cm^{-1} and for the Lorentz and polarization effects. The peak shapes were fitted with pseudo-Voigt functions and the backgrounds were fitted with seven-parameter polynomial functions over the whole 2θ range.

We have started the structure refinement of the α-phase with the atomic positions and ADPs borrowed from the structural model of berlinite [4]. Finally, the α-$FePO_4$ structure was refined with the reliability factor $R_p = 4.9\%$. For β-$FePO_4$, the x-ray diffraction diagram collected at $T = 1073$ K showed some peaks which could not be attributed within the symmetry group of β-$FePO_4$. Similarly, they could not be assigned to an admixture of the orthorhombic $FePO_4$ structure, another allotropic form of iron phosphate [26]. Thus, we concluded that a parasite phase probably appears as a result of atomic diffusion into the $FePO_4$ sample from the silica capillary tube. The determination of the space group and cell parameters of this parasite structure was performed by using the profile matching mode with a constant scale factor. This was done by using the x-ray reflections in the intervals in which there is no reflection from the $FePO_4$ itself. This led us to the conclusion that the parasite structure belongs to the space group $Pmmm$ with unit cell parameters $a = 17.444$ Å, $b = 9.558$ Å and $c = 8.436$ Å, which reduced the total reliability factor down to $R_p = 6.5\%$. Additional refinements have been tested to determine if the composition changes occur with the formation of the parasite phase. Full Rietveld refinement, with a linear constraint to keep the charge balance of the compound, converged on a stoichiometric composition

Table 2. Isotropic displacement parameters U_{iso} (in 10^{-2} Å^2) and reliability factor R_{Bragg} for α-and β-phases of $FePO_4$.

	α-phase, $T = 300$ K		β-phase, $T = 1073$ K	
	XRD, this work	ND, [5]	XRD, this work	ND, [5]
Fe	1.00(2)	0.79(3)	3.16(3)	3.1(2)
P	1.05(2)	1.01(4)	7.28(5)	5.3(4)
O1	2.02(1)	1.41(4)	13.15(5)	11.6(3)
O2	2.27(1)	1.24(4)		
R_{Bragg}	0.024	0.022	0.053	0.26

within the standard deviations. Careful refinements with and without the additional phase and only fixing the occupancy, the scale factor and atomic parameter, have been performed to see if the parasite phase has an influence on the IDP of the β-phase. No significant changes are observed within the error bars. ADP refinement with a model containing a single oxygen position decreased the reliability factor by about 1%. Similar results were obtained with split oxygen sites constraining the equal ADP/IDP for both O atoms, thus suggesting that both results are equivalent.

3.2. Experimental results

The structural parameters thus determined of both α-and β-$FePO_4$ are shown in table 1 in comparison with the ND results reported in [5].

All structural parameters of the α-phase determined by both experimental techniques are close to each other. The same is true for the positional parameters of the β-phase. The unit cell parameters of the β-phase lattice determined in our XRD study are slightly larger than those determined in [5].

Our structural refinement included determination of ADPs, which are defined as elements of the mean square displacement matrix $U_{ij} = \langle \Delta x_i \Delta x_j \rangle$. The equivalent IDPs, determined through the U matrix as $U_{iso} = \frac{1}{3}(U_{11}+U_{22}+U_{33})$, are presented in table 2 in comparison with the values reported in [5].

It is noticeable that the room-temperature U_{iso} values found for α-$FePO_4$ in [5] are rather close to those reported for $AlPO_4$ [22]. The U_{iso} values obtained in our XRD study are systematically larger than those reported in [5]. This excess is about 15% for all atoms in both α-and β-phases with the exception of oxygen atoms in α-$FePO_4$ for which the excess reaches 65%. Besides, our results and the results of [5] give different values for the ratio $U_{iso}(O1)/U_{iso}(O2)$: it is equal to 0.89 and 1.14, respectively.

In spite of these disagreements, the two experimental results show some coinciding trends which allow us to distinguish differences in behaviour of $FePO_4$ and $AlPO_4$. First of all, one should note that the increase of U_{iso} during the α–β transformation is much larger in $FePO_4$ than in $AlPO_4$. The data collected in table 2 show that the ratio of the U_{iso} values in the β-phase and α-phase is about 5 for both cation atoms, whereas this ratio is 3.6 in $AlPO_4$ [22]. The analogous ratio for oxygen atoms in $AlPO_4$ is 4.7 [22], whereas for $FePO_4$ it is equal to 6 or 9, according to ND and XRD data, respectively.

Consequently, all values of U_{iso} in β-$FePO_4$ are 1.6–1.9 times larger than in β-$AlPO_4$. This difference cannot be

Table 3. RMSDs (in Å) for A and B atoms in two phases of $FePO_4$ and $AlPO_4$.

		$FePO_4$, this work				$AlPO_4$ [22]	
		α-phase $T = 300$ K	β-phase $T =$ 1076 K			α-phase $T = 298$ K	β-phase $T = 904$ K
Fe	$R2$	0.120(1)	0.237(8)	Al	$R2$	0.0966	0.1975
	$R1$	0.099(1)	0.118(1)		$R1$	0.0875	0.1583
	$R3$	0.076(1)	0.157(8)		$R3$	0.0825	0.1567
P	$R2$	0.103(1)	0.151(2)	P	$R2$	0.0985	0.1831
	$R1$	0.118(1)	0.328(4)		$R1$	0.0867	0.1640
	$R3$	0.083(1)	0.256(1)		$R3$	0.0801	0.1692

explained by different temperatures of observation, because the U_{iso} values are almost temperature-independent in the β-phases of both compounds [5, 22]. This is the first important distinction between both compounds, which can be deduced from the analysis of IDPs.

Another noticeable difference between both compounds concerns the ratio $U_{iso}(A)/U_{iso}(B)$. In $AlPO_4$ it is close to unity at any temperature in both phases [22]. In $FePO_4$ this ratio is close to unity only in the α-phase. In the β-phase the ratio $U_{iso}(P)/U_{iso}(Fe)$ increases and reaches 2. This finding distinguishes $FePO_4$ from other quartz-type homologues, for which the relation $U_{iso}(A) \approx U_{iso}(B)$ was suggested as a family property and was explained by a strong A–O and B–O bonding in the two kinds of tetrahedra, which makes the effects of the different masses less important in the librations [22].

There should also be mentioned the remarkable difference between $AlPO_4$ and $FePO_4$ in the temperature variation of bond lengths. When comparing the bond lengths in the room-temperature α-phase structure and in the β-phase structure just above the SPT point, one can see that, according to [22], both Al–O and P–O bonds shorten by 2% and 8%, respectively. According to our data, the Fe–O bonds shorten by 7% whereas the P–O bonds lengthen by 3% at the SPT.

All the above-mentioned peculiarities allow us to suggest that the β-phase structure of $FePO_4$ is more disordered than in other quartz-like compounds, and this disorder mostly affects the PO_4 units. A deeper insight into the disordered nature of β-$FePO_4$ can be gained through the analysis of ADPs. It is convenient to characterize the anisotropy of ADPs by the lengths of the probability ellipsoid principal axes, the so-called root mean square displacements (RMSD), which are defined as the square roots of the eigenvalues of the U matrix.

In quartz-like ABO_4 structures, orientations of principal axes of the probability ellipsoids for A and B atoms are fixed by symmetry: one of them is directed along the twofold axis C_2, another one along the threefold axis C_3 and the third one along the C_1 axis which is perpendicular to C_2 and C_3. We denote the corresponding RMSDs as $R2$, $R3$ and $R1$, respectively. The parameters for the iron and phosphorus atoms derived from our experimental data are presented in table 3 in comparison with analogous data for $AlPO_4$.

Earlier it was found that $R2$ is the longest ellipsoid axis for A and B atoms in both phases of quartz [20] and berlinite [22]. Besides, the $R2$ value exhibits a sharp increase when passing the critical point. The $R1$ and $R3$ values are both smaller than $R2$; they are close to each other and change smoothly during the SPT.

The results presented in table 3 show that a similar behaviour is inherent in RMSDs of iron atoms in $FePO_4$. However, this is not the case for phosphorus atoms. According to our results, the longest ellipsoid axis for P atoms in both α- and β-phases is $R1$ but not $R2$. Moreover, $R2$ is the shortest ellipsoid axis for P atoms in β-$FePO_4$.

As a rule, the probability ellipsoids of oxygen atoms in the quartz-like ABO_4 crystals are represented within the coordinate system related to A–O–B angles. The three basis vectors are defined as follows. The vector **n**2 is directed along the bisector of the A–O–B angle, the vector **n**3 is perpendicular to the plane of the AOB angle and **n**1 is perpendicular to **n**2 and **n**3. In standard nomenclature used in vibrational spectroscopy, the oxygen atom oscillations along **n**1 are referred to as asymmetric A–O and B–O bond stretching. Normally, such vibrations are characterized by relatively high frequencies ($\sim$1000 cm^{-1}), hence by weak amplitudes. Oscillations along **n**2 correspond to symmetric A–O and B–O bond stretching mixed with the AOB angle bending. Such vibrations are usually of relatively lower frequency ($\sim$400 cm^{-1}), hence have higher amplitudes. The oscillations along **n**3 correspond to rotations of the A–O–B bridge around the A–B axis. They do not involve variations of 'rigid' internal coordinates—the bond lengths or AOB angle. Thus, they should have the lowest frequencies and the largest amplitudes.

According to [20, 22], these empirical common rules are perfectly fulfilled in quartz and berlinite: the ellipsoid axes of all O atoms, when listed in descending order, are oriented along the **n**3, **n**2 and **n**1 axes at all temperatures. According to our data, orientations of the probability ellipsoids for O atoms in $FePO_4$ do not obey (or even partly contradict) these rules. To describe quantitatively the orientations of these ellipsoids, we introduced the coefficients $c_{ij} = (\mathbf{e}_i \mathbf{n}_j)$, where $\mathbf{e}_i$ is the unit vector in the direction of the ith ellipsoid axis. Taking into account that $\sum_j c_{ij}^2 = 1$, one can consider the quantity $100c_{ij}^2$ as a percentage of the jth direction in the ith ellipsoid axis. These coefficients for all oxygen probability ellipsoids are represented in table 4.

One can see that in the α-phase the shortest ellipsoid axes, $R3$, for both O1 and O2 are directed presumably along **n**1 in good agreement with the common rule. At the same time, the longest ellipsoid axis, $R1$, is directed presumably along **n**2 but not along **n**3, as could be expected according to the above mentioned common rules.

Table 4. Lengths and orientations of ADP ellipsoid axes for O atoms in α-and β-$FePO_4$.

Atoms		RMSD (Å)	$100c_{ij}^2$ n1	n2	n3
O1 (α-phase)	$R1$	0.173(1)	0	99	0
	$R2$	0.153(2)	15	0	85
	$R3$	0.087(3)	84	1	15
O2 (α-phase)	$R1$	0.186(3)	24	58	18
	$R2$	0.170(1)	6	34	60
	$R3$	0.071(3)	70	8	22
O (β-phase)	$R1$	0.47(3)	89	11	0
	$R2$	0.31(2)	1	9	90
	$R3$	0.28(3)	12	78	10

According to our experimental data, the longest ellipsoid axis, $R1$, for O atoms in β-$FePO_4$ is directed along **n**1 rather than along **n**3 as it takes place in quartz and berlinite, and the shortest one presumably along **n**2 (not along **n**1 as it takes place in quartz and berlinite). It is worth noting that, according to our results, the ADP ellipsoids of O atoms in $FePO_4$ have the shape of lenses: the lengths of two longer axes ($R1$ and $R2$) are close to each other, and these axes are almost markedly longer than the shortest one ($R3$). This differs from results reported for quartz and berlinite, where the differences $R1 - R2$ and $R2 - R3$ were found to be almost equal at all temperatures.

These results might indicate that the probability distribution for O atoms in β-$FePO_4$ is dictated not by atomic oscillations localized within AOB bridges (this assumption is at the heart of the common rules), but rather by positional disorder related to the complex multi-domain structure of this phase or to low-frequency framework vibrations.

In order to verify this suggestion, we have refined the structure of β-$FePO_4$ assuming doubly split O positions. Thus we obtained two non-equivalent oxygen positions OI (0.416, 0.260, 0.565) and OII (0.427, 0.196, 0.615) with equal occupation numbers 0.5. These positions are separated by 0.68 Å. Deviations of OI and OII from the O position obtained for the ordered β-phase structure are not equivalent. However, both vectors **x**(OI)–**x**(O) and **x**(OII)–**x**(O) are almost collinear with the O-displacements dictated by the eigenvector of the classical soft mode [1], i.e. they are almost parallel to **n**3.

A fragment of the β-$FePO_4$ crystal structure with doubly split O positions is shown in figure 1. All studies of the α–β transformation in quartz-like ABO_4 crystals agreed that the A–O–B bridges are conserved during the transformation. Guided by this notion, we have tried to derive a microscopic interpretation for the β-$FePO_4$ structure with the doubly split oxygen positions. Two alternative interpretations were found. The first one, schematically depicted in figure 1(a), assumes that the split configurations are related to each other by concordant rotations of all FeO_4 and PO_4 tetrahedra around C_2 axes. This is just what is dictated by the eigenvector of the classical soft-mode model. In this case, the P and Fe atoms should move along the C_2 axes, thus leading to ADP ellipsoids mostly elongated in these directions. This is the case for quartz and berlinite.

An alternative interpretation, presented in figure 1(b), implies that the split configurations come from rotations of

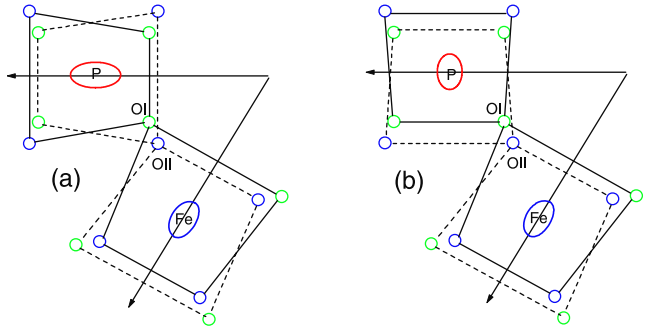

Figure 1. Possible arrangements of PO_4 and FeO_4 tetrahedra in β-$FePO_4$ structure consistent with split O position model: (a) tetrahedra rotate around $C2$ axes and (b) rotational axes are perpendicular to $C2$ axes. The $C2$ axes are shown by arrows. Two equivalent tetrahedra orientations are shown by solid and dashed lines. Corresponding ATP ellipsoids of P and Fe atoms are shown by ellipses.

FeO_4 tetrahedra around C_2 axes accompanied by concordant rotations of PO_4 tetrahedra around C_1 axes. Such a distortion can also be accomplished without significant deformation of P–O–Fe bridges. In this case, the Fe and P atoms move along the axes of corresponding tetrahedra rotations, i.e. along the C_2 and C_1 axes, respectively. This inevitably results in different shapes of the ADP ellipsoid for Fe and P atoms which would have the longest axes $R2$ and $R1$, respectively. This mechanism may explain our experimental results on ADPs.

Both patterns of atomic displacements shown in figures 1(a) and (b) involve tetrahedra rotations and translations. The requirement that they correspond to a phonon mode of low frequency implies that they must preserve the integrity of the framework built up of the corner-sharing tetrahedra. From this condition it can be deduced that the atomic displacements shown in figure 1(a) must correspond to a zone-centre phonon mode, and that shown in figure 1(b) must belong to a zone-edge phonon mode with wavevector $(0, 0, 1/2)$. Which of the two modes gives a predominant contribution to APDs in β-$FePO_4$ depends on their relative stability (or rather instability).

4. Lattice dynamics analysis

In order to clarify this issue, we performed lattice dynamics simulations and analysed the whole set of low-frequency phonon modes which give the highest contributions to the atomic thermal amplitudes in β-$FePO_4$. To the best of our knowledge, there was one attempt at direct lattice dynamics simulations in $FePO_4$ based on an empirical potential model proposed by Mittal *et al* [27]. This model does not seem appropriate for our purposes because of two reasons. First, it predicts IADs of Fe atoms larger than those of P atoms at all temperatures [27]. This evidently contradicts the experimental observation. Second, this model was developed assuming transferability of the ionic charges and the P–O and the O–O pair-wise short-range potentials between $AlPO_4$ and $FePO_4$. Thus, this model *a priori* implies a close similarity between the two compounds. This seems quite doubtful

because the electronic cloud of the Fe^{3+} ion is an open-shell system with partially occupied d-orbitals. Consequently, the $[Al(OH)_4]^{1-}$ cluster used for the evaluation of potential model parameters in $AlPO_4$ [28], is not appropriate for $FePO_4$. Indeed, the quantum-mechanical study of different clusters containing Fe–O–P bridges [29] and Al–O–P bridges [30] revealed essential differences in their electronic structures. In this connection, it is worth noting that the high flexibility of the electronic structure of iron atoms connected to phosphate groups manifests itself in a large variability of the FeO_n polyhedra, with the coordination number of the Fe^{3+} atoms changing from 3 to 7 [29]. This peculiarity can hardly be adequately taken into account in a simple potential model based on pair-wise interactions with fixed atomic charges.

These objective difficulties forced us to choose a simpler but more reliable approach. First of all, we analysed the set of low-energy vibrations that are allowed to be excited in β-$FePO_4$ as a result of the symmetry change induced by the phase transition, as was suggested in [24]. It was shown that these low-frequency vibrations are closely related to rigid unit modes (RUM) [31]. The RUMs are phonon modes in which the tetrahedra move as rigid units without distorting significantly. Many of the RUMs have very low frequencies; many of them become harmonically unstable in the β-phase [32]. Low frequencies lead to large amplitudes. This means that the large amplitude tetrahedra rotations and displacements in the β-phase configuration are primarily due to the excitation of RUMs. Calculations have shown that there are significantly more RUMs in the β-phase than in the α-phase [31]. This fact is due to the geometry change associated with the phase transition. As a consequence, some modes which were pure tetrahedra rotations in the β-phase inevitably involve some degree of tetrahedra deformations in the α-phase.

The whole set of RUMs in β-quartz was analysed in [31]. Here we briefly summarize these results. It was shown that RUMs are distributed in the Brillouin zone (BZ) of a quartz-like AO_2 lattice as is shown in figure 2(a). One can consider the berlinite-like ABO_4 lattice as derived from the AO_2 lattice by the alteration of atoms A and B in the neighbouring cation positions. Such alteration leads to the doubling of the unit cell in the c direction. Correspondingly, the BZ of the ABO_4 lattice can be represented as a result of a folding of the BZ of the AO_2 lattice at the (0 0 1/4) plane. Thus one can expect the presence of 6 RUM branches in the Γ–A direction and two RUM branches in the Γ–M and Γ–K directions for the β-phase of the ABO_4 lattice as is schematically shown in figure 2(b).

Analysis of atomistic patterns of eigenvectors corresponding to different RUMs allowed us to reveal the RUMs mostly affecting the anisotropy of the ADP ellipsoid. For the β-AO_2 structure these RUMs are shown in figure 3. Below we label these RUMs by one letter, which indicates the corresponding BZ point, and by one index which enumerates the RUMs belonging to the same BZ point. Thus, we have one Γ-RUM (see figure 3(a)), which plays a role of the soft mode for the classical model of displacive α–β phase transition (cf figures 1(a) and 3(a)). Three other Γ-RUMs are conventional translations giving rise to three acoustic branches. Besides, we have three A-RUMs, two of which are doubly degenerated. A non-degenerated A-RUM and one component of the doubly degenerated A-RUMs are shown in figures 3(b) and (c). In fact, all A-modes imply alteration of the displacements of atoms translated along the z axes by the vector **c**. This should be taken into account in considering figures 3(b) and (c) in which the z positions of tetrahedra are given by small numbers. Finally, we have two M-RUMs as shown in figures 3(d)–(f). One can see that these modes primarily consist of rotations of the tetrahedra. The only exception concerns the M1-mode (see figure 3(d)) in which half of the tetrahedra execute pure translations. It should be pointed out that, as a rule, rotations of tetrahedra are accompanied by their translations along the rotational axis. This fact is due to the condition of preservation of the integrity of the framework, and is especially pronounced in the cases of the Γ-RUM and A1-RUM. Directions of the tetrahedra translations coincide with the rotational axes shown in figure 3 by thin arrows.

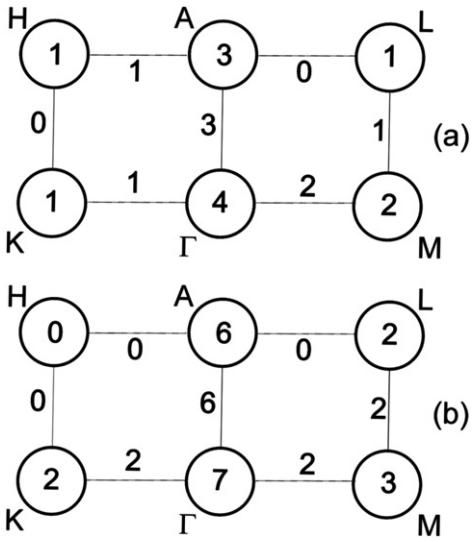

Figure 2. Distribution of RUMs within the BZ of β-AO_2 (a) and β-ABO_4 (b) crystals. Numerals in circles and on lines show the number of RUMs in special points and along symmetric directions of the BZ, respectively.

The existence of two M-RUMs in β-quartz was confirmed experimentally in the neutron diffraction experiments [33]. The measured frequencies were about 33 and 58 cm^{-1} for the M1- and M2-modes, respectively. It was suggested that softness of the two Γ–M phonon branches plays an important role in formation of the multi-domain twin structure and diffuse scattering observed near the phase transition. Possible participation of the A1-RUM in the dynamic disordering of β-quartz was first suggested in [34]. The predicted frequency of this mode near the transition point was about 20 cm^{-1}.

When interested in revealing the modes which determine anisotropy of the ADPs of A atoms (the centres of tetrahedra), one should focus upon three modes, Γ-RUM, A1-RUM and M1-RUM, which involve tetrahedra translations in the xy plane. There are three M-points in the BZ. Correspondingly, there are three M1-RUMs (similar to those shown in figure 3(d)) with translational motions along the (100), (010) and (110) crystallographic directions. Hence, these modes

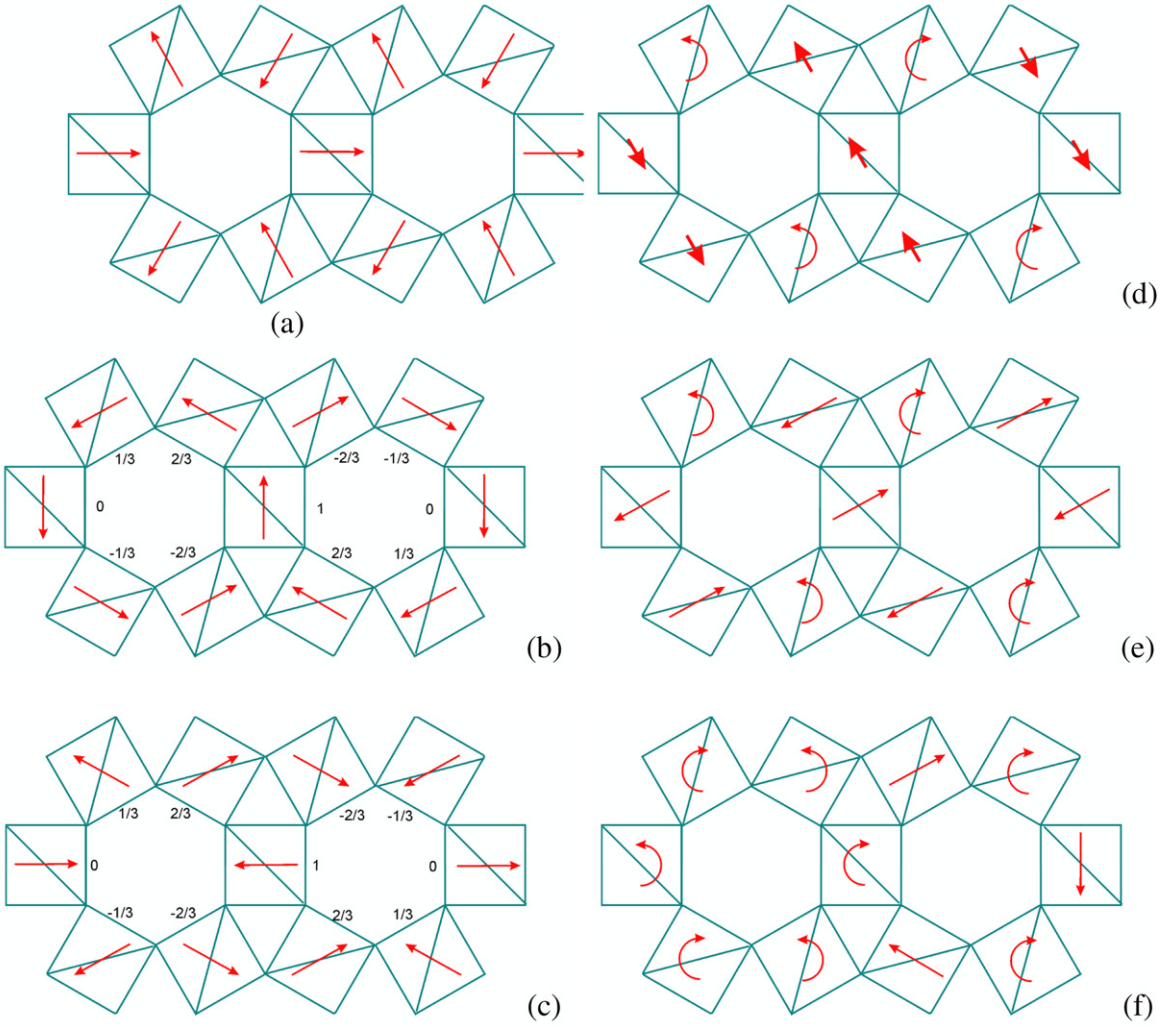

Figure 3. Shapes of different RUMs in β-quartz: Γ-RUM (a), A1-RUM (b), A23-RUM (c), M1-RUM (d), M2-RUM (e) and K-RUM (f). Curved arrows show directions of tetrahedra rotations around axes parallel to z, long and thin arrows show directions of rotational axes lying in the xy plane and thick arrows show translations of tetrahedra in the xy plane. Small numbers in (b) and (c) indicate positions of tetrahedra along the z axis.

do not contribute to the anisotropy of ADPs in the xy plane. Contrariwise, the Γ-RUM and A1-RUM evidently affect this anisotropy. The former mode involves the tetrahedra translations along the C_2 axes, and the latter mode in the perpendicular direction, i.e. Γ-RUM and A1-RUM mostly contribute to $R2$ and $R1$ values, respectively. Experimental studies of lattice dynamics in β-quartz revealed the soft-mode behaviour for Γ-RUM: the frequency of this mode vanishes on approaching the critical point [35]. At the same time, no soft mode was found in the A-point. This is in agreement with other experimental data [20] where the estimate of the $R2$ value is markedly larger than $R1$.

This model works equally well for quartz and berlinite, even if another BZ direction (Γ–A) contains three times more RUMs. This phenomenon takes place because the Γ-RUM softens on approaching the critical point much more rapidly than other RUMs. This result is closely related to the condition that both AO_4 and BO_4 tetrahedra are of about the same rigidity. This is not the case for $FePO_4$. In view of the markedly longer Fe–O bonds, one can suggest that the FeO_4 tetrahedra must be essentially softer than PO_4 tetrahedra. This particularity of $FePO_4$ may cause important changes in the low-frequency part of the phonon spectrum and, consequently, in the shape of ADP ellipsoids in comparison with other quartz-like crystals. Below, we advance some quantitative arguments in favour of this suggestion.

Due to folding of the BZ, the modes belonging to the A-point in the quartz-like AO_2 lattice transform into zone-centre modes in the berlinite-like ABO_4 lattice, and the phonons belonging to the (0 0 1/4) point in the AO2 lattice transform into A-phonons in the ABO_4 lattice. Thus, in Γ and A points of the β-ABO_4 lattice there are seven and six RUMs, respectively. Only four of them affect the anisotropy of tetrahedra translations. Two such modes come from the Γ-RUM and A-RUM of the AO_2 lattice. Both of them belong to the Γ-point in the ABO_4 structure; below, we shall refer to them as $\Gamma1$ and $\Gamma2$. Two other RUMs originate from (0 0 1/4) phonons of the AO_2 lattice and belong to the A-point

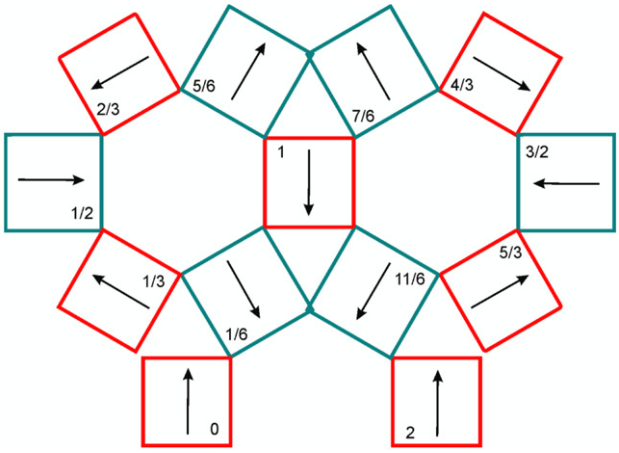

Figure 4. Fragment of β-$FePO_4$ structure in xy projection. Contours FeO_4 and PO_4 tetrahedra are shown by blue and red squares. The z positions of the centres of tetrahedra are given by small numbers. Arrows show axes of the tetrahedra rotations corresponding to A(Fe)-RUM.

in the ABO_4 structure. They are of particular interest, because they involve atomic displacements which lead to a different anisotropy of ADPs for A and B atoms. One of these modes is shown in figure 4. It can be seen that in this mode all AO_4 tetrahedra rotate around the C_2 axes and all BO_4 tetrahedra rotate around the C_1 axes. We have the inverse situation in the second mode: the BO_4 tetrahedra rotate around the C_2 axes and the AO_4 tetrahedra rotate around the C_1 axes. We shall refer to these two modes as A(A) and A(B) modes, respectively. Recall that in both modes the tetrahedra rotations are accompanied by translational motions along the axes of rotation. Thus, the large amplitude of the A(A) mode results in APD ellipsoids of A and B atoms elongated along the C_2 and C_1 axes, respectively.

It should be emphasized that namely the large amplitude of the A(A)-mode is at the heart of our hypothesis, which could provide an explanation of the anisotropy of ADPs observed in our experiments on $FePO_4$. In order to justify this hypothesis, we have to show that A(A)-RUM actually is one of the softest modes in β-$FePO_4$.

Now we turn to quantitative estimation of the frequencies of different RUM-like modes in β-$FePO_4$. When going beyond the RUM approximation, one should take into account the finite rigidity of the AO_4 and BO_4 tetrahedra and the long-range inter-tetrahedra interactions. We have simulated the phonon spectrum of the ABO_4 crystals with the use of a simple potential model, which takes into account both factors.

The dynamic matrix includes two contributions. The first one, corresponding to the A–O and B–O bond stretching deformations, was described by harmonic bond stretching potentials

$$U = \tfrac{1}{2}\sum_n \sum_{i=1}^{4} K_n (R_{ni} - R_n^0)^2,$$

where R_{ni} is the simultaneous length of the ith bond in the nth tetrahedron, R_n^0 is the equilibrium value of the bond lengths and K_n are corresponding force constants. Values of R_n^0 were chosen as lengths of the A–O and B–O bonds in the room-temperature a-structure. Values of K_n were fitted to reproduce

Table 5. Model parameters and frequencies (in cm^{-1}) of some phonon modes for the α-phase structures.

ABO_4	R_A^0, R_B^0 (Å)	K_A, K_B (N m^{-1})	$\nu1$, $\nu2$ (calc.)	$\nu1$, $\nu2$ (exp.)
SiO_2	1.609	360	1068, 469	1080, 464 [37]
$AlPO_4$	1.735, 1.523	320, 475	1107, 464	1112, 461 [38]
$FePO_4$	1.850, 1.542	180, 440	1015, 412	1015, 405 [36]

frequencies of the two modes observed in Raman spectra of the ABO_4 crystals. The first of them ($\nu1$) involves the anti-phase pulsations of the AO_4 and BO_4 tetrahedra and the second one ($\nu2$) involves in-phase stretching of A–O and B–O bonds within all A–O–B bridges. Frequencies of both these modes are rather sensitive to the bond stretching force constants.

The second term of the dynamical matrix corresponds to O–O pair-wise interactions which determine the rigidity of the AO_4 and BO_4 tetrahedra with respect to bending deformations, as well as the inter-tetrahedra interactions. Interaction between mth and nth O atoms was described by Born's longitudinal pair-wise force constants $A_{mn} = \frac{\partial^2 U}{\partial r_{mn}^2}$. These quantities were assumed to depend on O–O distance $r_{mn} = |x_m - x_n|$ according to the relation

$$A_{mn} = A_0 \exp\left(-\frac{r_{mn}}{\rho}\right).$$

The parameter $\rho = 0.36$ Å was chosen as an average of values used in other previously published potential models [21, 23, 28, 29]. The parameter $A_0 = 1.2 \times 10^5$ N m^{-1} was fitted so that the low-frequency parts of the optical phonon spectra cover the frequency interval between 100 and 400 cm^{-1} in accordance with experimental data [36].

It should be emphasized that there are only three fitting parameters K_{AO}, K_{BO} and A_0. Besides, the A_0 value was assumed to be equal for all compounds under study. Estimated values of the model parameters are presented in table 5 along with calculated frequencies which are compared with experimental data. Note that the values of force constants used in our model decrease monotonically with bond length and are in agreement with the values used in more sophisticated valence force field models [37, 39].

We have used this defined potential model to calculate phonon spectra for β-phase structures of three compounds: SiO_2, $AlPO_4$ and $FePO_4$. The structural parameters for β-quartz and β-berlinite were taken from experimental data [20, 22] and for β-$FePO_4$ from table 1. The calculated frequencies of the RUM-related modes are shown in table 6. It is seen that many of them take imaginary values. This result can be explained as follows.

The phonon states in the low-frequency part of the spectrum are very sensitive to structural variations during the α–β transformation. First of all, this is due to kinematical reasons mentioned above: some modes involving intra-tetrahedra deformations in the α-phase become pure RUMs in the β-phase. The second reason is related to the bond length variation. It was well established that both A–O and B–O bonds shorten markedly in the β-phase. This bond shortening induces intra-tetrahedral tensions which produce a

Table 6. Bond lengths in β-phase structures and calculated frequencies (in cm^{-1}) of RUMs.

ABO_4	R_A, R_B (Å)	Γ1-RUM	Γ2-RUM	A(A)-RUM	A(B)-RUM
SiO_2	1.5624	83i	28i	82i	82i
$AlPO_4$	1.7091, 1.4902	58i	43	34i	38i
$FePO_4$	1.7128, 1.5850	38i	27	19i	22

destabilizing effect on the modes involving rotations of the tetrahedra [40]. As a consequence, many of the rotational modes become harmonically unstable. This means that corresponding oscillations are no longer described by a single-minimum potential but by a double-minimum potential well [39]. Namely, these modes having imaginary values of harmonic frequencies contribute mostly to the thermal atomic amplitudes. The greater is the imaginary part of the frequency the higher is this contribution.

Comparing tables 5 and 6, one can see that all A–O and B–O bonds become shorter in the β-phase than in the α-phase in quartz and berlinite. The bond reduction is equal to 0.047, 0.025 and 0.033 Å for the Si–O, Al–O and P–O bonds, respectively. All these valence bonds are rather rigid as can be judged from the force constant values cited in table 5. Therefore, shortening of these bonds induces significant internal tensions in all the tetrahedra. Due to this all considered RUMs become harmonically unstable.

It is seen that in β-quartz all the RUMs have imaginary harmonic frequencies. The most unstable are Γ1, A(A) and A(B). It should be mentioned that in quartz, in which A and B atoms are identical, the frequencies of A(A) and A(B)-RUMs are equal by symmetry. It is remarkable that these frequencies are almost equal in β-$AlPO_4$ too. So, these modes, having almost equal amplitudes, cannot lead to different anisotropy of ADPs for Al and P atoms. For both β-quartz and β-berlinite this anisotropy is caused by a difference in frequency between Γ1-RUM and Γ2-RUM. The former is more unstable. This results in ADP ellipsoids elongated along the C_2 axes for all cation atoms in β-SiO_2 and β-$AlPO_4$.

The situation is different in β-$FePO_4$. Our calculations revealed a significant difference between A(Fe)-RUM and A(P)-RUM. The latter mode is harmonically stable, whereas the A(Fe)-RUM is unstable with an imaginary frequency quite comparable with the frequency of the Γ1-RUM. One can see that atomic displacements corresponding to this mode are close to those dictated by a structural model with disordered O positions derived from our experimental data (cf figures 1(b) and 4).

In view of the results presented in table 6, one can conclude that the anisotropy of the ADP ellipsoids of Fe P atoms results from concurrent contributions of the two harmonically unstable modes, Γ1-RUM and A(Fe)-RUM. The prevalence of the former would lead to ADP ellipsoid shapes for Fe and P atoms similar to those in quartz and berlinite. The prevalence of the latter would result in the anisotropy of those ellipsoids which follows from our experimental data. We are inclined to believe that the second supposition is more likely, even if the imaginary frequency of Γ1-RUM is larger than that of A(Fe)-RUM. This conclusion, derived from calculations based on a simple potential model, provides a justification for our hypothesis and sheds some light on the rather unusual experimental results showing a significant difference in anisotropy of ADPs for Fe and P atoms in $FePO_4$.

5. Conclusions

The peculiar properties of $FePO_4$ were ascribed to the Fe cation being a transition metal. As a consequence of the partially occupied d-orbitals, it is proportionally larger than the closed-shell cations of groups IIIA–IVA. After the conclusion issued in [5], that the behaviour of this material differs from that observed in quartz and berlinite, we confirm that structural and dynamical properties in $FePO_4$ distinguish themselves from those in quartz and berlinite. The magnitude of the β-to-α structural distortion in α-$FePO_4$ at room temperature is confirmed in the present study to be larger than in SiO_2 and $AlPO_4$ and closer to values typical for compounds which do not exhibit α–β transitions (GeO_2, $GaPO_4$, $AlAsO_4$, $GaAsO_4$). Moreover, the spontaneous discontinuity of structural parameters at T_c is stronger in $FePO_4$ than in SiO_2 and $AlPO_4$. These facts, in the authors' opinion, may indicate that the instability in $FePO_4$ has a dynamical nature. The dissimilarity of $FePO_4$ from quartz and berlinite is also found in the features of the deduced ADPs; the approach in terms of RUMs allows understanding the characteristics of the dynamical disorder and their thermal change.

After a long period when it was assumed that the problem of the SPT could be completely solved and understood from the Landau theory analysing the symmetry breaking, and the fluctuation theories, including the renormalization group theory approach, more detailed experimental studies, such as the present one, exhibit features more complex than those admitted to hold in the above schemes. Details of the structure of the system are necessary to understand the dynamics, and the relevant dynamics itself is not necessarily resumed by the critical fluctuations of the order parameter.

Acknowledgments

We thank the Conseil Regional Languedoc Roussillon that provided the financial support for the invitation of one of us (MS) to Nîmes University.

References

[1] Grimm H and Dorner B 1975 *J. Phys. Chem. Solids* **36** 407
[2] Ng H and Calvo C 1976 *Can. J. Phys.* **54** 638
[3] Kosten K and Arnold H 1980 *Z. Kristallogr.* **152** 119
[4] Goiffon A, Jumas J C and Philippot E 1986 *Rev. Chim. Miner.* **23** 99
[5] Haines J, Cambon O and Hull S 2003 *Z. Kristallogr.* **218** 193
[6] Dolino G 1981 *Phase Transit.* **21** 59
[7] Aslanyan T A, Shigenari T and Abe K 1998 *J. Phys.: Condens. Matter* **10** 4577
[8] Saint-Grégoire P, Snoeck E and Aliouane N 2001 *Ferroelectrics* **252** 1
[9] Yakovlev I A, Mikheeva L F and Velichkina T S 1956 *Sov. Phys.—Cryst.* **1** 91
[10] Shapiro S M and Cummins H Z 1968 *Phys. Rev. Lett.* **21** 1578

[11] Dolino G 1980 *Phys. Status Solidi* a **60** 391
[12] Cummins H Z and Levanyuk A P 1983 *Light Scattering Near Phase Transitions* (Amsterdam: North-Holland) p 605
[13] Dolino G, Mogeon F and Soula V 1991 *Phase Transit.* **36** 129
[14] Saint-Grégoire P *et al* 1996 *JETP Lett.* **64** 376
[15] Aliouane N *et al* 2000 *Ferroelectrics* **24** 255
[16] Dolino G, Bachheimer J P and Zeyen C 1983 *Solid State Commun.* **45** 295
[17] Gouhara K, Li Y H and Kato N 1983 *J. Phys. Soc. Japan* **52** 3697
[18] Bachheimer J P *et al* 1984 *Solid State Commun.* **51** 55
[19] Durand J, Lopez M, Cot L and Saint-Gregoire P 1983 *J. Phys.: Condens. Matter* **16** 311
[20] Kihara K 1990 *Eur. J. Mineral.* **2** 63
[21] Tsuneyuki S, Aoki H and Tsukada M 1990 *Phys. Rev. Lett.* **64** 778
[22] Muraoka Y and Kihara K 1997 *Phys. Chem. Miner.* **24** 243
[23] Kihara K and Matsui M 1999 *Phys. Chem. Miner.* **26** 601
[24] Tucker M G, Dove M T and Keen D A 2000 *J. Phys.: Condens. Matter* **12** L723
[25] Rodriguez-Carvajal J 1993 *Physica* B **192** 55
[26] Eventoff W, Martin R and Peacor D R 1972 *Am. Mineral.* **57** 45
[27] Mittal R, Chaplot S L, Kolesnikov A I, Loong C K, Jayakumar O D and Kulshreshtha S K 2002 *Phys. Rev.* B **66** 174304
[28] Kramer G J, Farragher N P, van Beest B W H and Santen R A 1991 *Phys. Rev.* B **43** 5068
[29] Dhouib A, Minot C and Abderrab M 2008 *J. Mol. Struct. THEOCHEM* **860** 161
[30] Ignatyev I S and Sundius T 1999 *J. Mol. Struct. THEOCHEM* **480/481** 667
[31] Hammonds K D, Dove M, Giddy A P, Heine V and Winkler B 1996 *Am. Mineral.* **81** 1057
[32] Smirnov M B 1999 *Phys. Rev.* B **59** 4036
[33] Boysen H, Dorner B, Frey F and Grimm H 1980 *J. Phys.: Condens. Matter* **13** 6127
[34] Kihara K 1993 *Phys. Chem. Miner.* **19** 492
[35] Tezuka Y, Shin S and Ishigame M 1991 *Phys. Rev. Lett.* **66** 2356
[36] Pasternak M P *et al* 1997 *Phys. Rev. Lett.* **79** 4409
[37] Mirgorodskii A P 1980 *Opt. Spektrosk.* **48** 183
[38] Gregora I, Magneron N, Simon P, Luspin Y, Raimboux N and Philippot E 2003 *J. Phys.: Condens. Matter* **15** 4487
[39] Mazhenov N A, Smirnov M B and Shchegolev B F 1992 *Opt. Spektrosk.* **72** 129
[40] Mirgorodsky A P and Smirnov M B 1994 *Ferroelectrics* **159** 133